

Fisher Curvature Scaling at Critical Points: An Exact Information-Geometric Exponent from Periodic Boundary Conditions

Max Zhuravlev¹

¹*Independent Research**
(Dated: March 10, 2026)

We study the scalar curvature R of the Fisher information metric on the microscopic coupling-parameter manifold of lattice spin models at criticality. For a d -dimensional lattice with periodic boundary conditions (PBC) and $n = L^d$ sites, the Fisher manifold has $m = d \cdot n$ dimensions (one per bond), and we find $|R(J_c)| \sim n^{d_R}$ with

$$d_R = \frac{d\nu + 2\eta}{d\nu + \eta},$$

where ν and η are the correlation-length and anomalous-dimension critical exponents. For the 2D Ising universality class ($\nu = 1$, $\eta = 1/4$), this predicts $d_R = 10/9 = 1.1\bar{1}$, confirmed by exact transfer-matrix computations ($L = 6-9$: $d_R = 1.1115 \pm 0.0002$, 1.8σ) and multi-seed MCMC through $L = 24$ (all effective exponents within 2.2σ). For 3D Ising ($\nu = 0.630$, $\eta = 0.0363$), the prediction $d_R = 1.0188$ is consistent with MCMC results on L^3 tori up to $L = 10$ (power-law fit $L = 5-10$: $d_R = 1.040$). For 2D Potts $q = 3$ (predicted $d_R = 33/29 \approx 1.138$), FFT-MCMC through $L = 40$ shows d_{eff} oscillating non-monotonically around ~ 1.20 for $L = 14-40$, consistent with $O(1/(\ln L)^2)$ logarithmic corrections. For $q = 4$ (predicted $d_R = 22/19 \approx 1.158$), effective exponents oscillate around ~ 1.28 for $L = 6-36$ with growing error bars at $L \geq 24$ ($\sigma \sim 0.05-0.10$), consistent with strong logarithmic corrections from the marginal $c = 1$ operator. The Ricci decomposition identity $R_3 = -R_1/2$, $R_4 = -R_2/2$ holds to 5–6 digits for all models and system sizes, providing a structural consistency check. For all second-order transitions studied, we find the statistical manifold at criticality to be hyperbolic (negative scalar curvature) under periodic boundary conditions. This exponent is distinct from the Ruppeiner thermodynamic curvature ($|R_{\text{Rup}}| \sim \xi^d$) and reflects the collective geometry of the growing $m \sim L^d$ dimensional Fisher manifold. We provide falsification criteria and predictions for additional universality classes.

INTRODUCTION

Information geometry provides a natural Riemannian structure on families of probability distributions [2, 4]. In statistical mechanics, the *Ruppeiner metric*—defined on the thermodynamic state space (T, h, \dots) —yields a scalar curvature that diverges as $|R| \sim \xi^d$ near a second-order phase transition, where ξ is the correlation length and d the spatial dimension [1, 3]. This identification of curvature with correlation volume has been confirmed analytically for the 2D Ising model [5] and numerically for various systems, including the quantum field-theoretic setting [6].

A complementary but distinct Riemannian manifold arises when one considers the *microscopic* coupling space. For a lattice model on graph $G = (V, E)$ with $|E| = m$ edge couplings $\{J_e\}_{e \in E}$, the Fisher information matrix

$$F_{ab} = \text{Cov}(\sigma_a, \sigma_b), \quad \sigma_e = s_i s_j \quad (e = ij), \quad (1)$$

defines an m -dimensional Riemannian metric on the space of couplings. This metric encodes the full correlation structure of bond observables and in general differs from the Ruppeiner metric, which lives on a lower-dimensional thermodynamic manifold.

In this Letter we compute the scalar curvature R of the m -dimensional Fisher manifold (1) at the bulk critical coupling for Ising and Potts models on lattices with

periodic boundary conditions (tori). We find a power-law divergence $|R(J_c)| \sim n^{d_R}$ and derive the formula for the exponent $d_R = (d\nu + 2\eta)/(d\nu + \eta)$ in terms of standard critical exponents. The curvature formulas used here are developed in the companion paper [7], which also proves the Riemann tensor decomposition identity that underlies the scalar Ricci identity exploited throughout.

SETUP

Model. Consider the Ising model on an $L \times L$ square lattice (or L^d hypercubic lattice in d dimensions) with *periodic* boundary conditions (torus), $n = L^d$ vertices, and $m = d \cdot L^d$ bonds. The partition function at uniform coupling $J_e = J$ is $Z(J) = \sum_{\{s\}} \exp(J \sum_{e \in E} s_i s_j)$. Each bond observable $\sigma_e = s_i s_j \in \{-1, +1\}$ and the Fisher metric (1) is an $m \times m$ positive-definite matrix. We compute results via exact transfer matrix (TM) for 2D models ($L \leq 9$), multi-seed Wolff-cluster MCMC with FFT cumulant accumulation for 2D at $L = 10-24$, GPU-accelerated MCMC with translational symmetry averaging (symavg) for 3D models ($L \leq 9$), and a two-phase pipeline (chunked MCMC sampling followed by GPU/CPU curvature assembly with jackknife error estimation) for 2D Potts at $L = 24-36$.

Curvature. The scalar curvature of a Riemannian manifold (M, g) is $R = g^{ac}g^{bd}R_{abcd}$, where R_{abcd} is the Riemann tensor constructed from the Christoffel symbols $\Gamma_{ab}^c = \frac{1}{2}g^{cd}(\partial_a g_{bd} + \partial_b g_{ad} - \partial_d g_{ab})$. We compute these derivatives via the third cumulant

$$\kappa_{abc} = \langle (\sigma_a - \mu_a)(\sigma_b - \mu_b)(\sigma_c - \mu_c) \rangle, \quad (2)$$

from which $\partial_c F_{ab} = \kappa_{abc}$ and the Christoffel symbols follow directly. Explicit closed-form curvature expressions in terms of F_{ab} and κ_{abc} are given in [7].

Ricci decomposition. The companion paper [7] establishes the Riemann tensor decomposition identity $R^a{}_{bcd}|_{\text{lin}} = -2R^a{}_{bcd}|_{\text{quad}}$ for cycle graphs (analytically) and verifies it across 42 graph families including all single-block discrete exponential families tested. As a scalar consequence numerically verified throughout this work, the curvature satisfies the Ricci identity

$$R_3 = -\frac{1}{2}R_1, \quad R_4 = -\frac{1}{2}R_2, \quad (3)$$

where $R = R_1 + R_2 + R_3 + R_4$ decomposes scalar curvature into contractions involving zero, one, two, and three inverse-metric factors in the Christoffel-symbol products. The identity implies $R = (R_1 + R_2)/2$, so only two independent Ricci scalars need to be computed. We verify (3) to 5–6 significant figures for all models and sizes reported here, confirming the integrity of the numerical pipeline.

Distinction from prior work. The Ruppeiner curvature R_{Rup} is computed on the 2-dimensional thermodynamic manifold (T, h) and diverges as $|R_{\text{Rup}}| \sim |t|^{-d\nu}$ near the critical temperature, where $t = (T - T_c)/T_c$ [1, 5]. Recent work [6] extends the analysis to the 2D *uniform* coupling space (J, K) , but the manifold dimension remains fixed at 2. Machta et al. [11] studied the eigenvalue spectrum of the Fisher matrix in multi-parameter coupling spaces but did not compute geometric invariants such as scalar curvature. Campos Venuti and Zanardi [17] showed that the fidelity susceptibility—which is the trace of the quantum geometric tensor—diverges at quantum phase transitions with an exponent set by ν , establishing information geometry as a probe of criticality. Prokopenko et al. [18] related Fisher information to classical order parameters, while Lima et al. [19] recently proposed a geometrical interpretation of η through fractal dimensionality at criticality. Our curvature is computed on the m -dimensional microscopic coupling manifold (one parameter per bond), where $m = d \cdot L^d$ grows with system size. The divergence is measured as a function of L at fixed $J = J_c$. These are fundamentally different geometric objects.

RESULTS

2D Ising: Definitive Confirmation of $d_R = 10/9$

The 2D Ising model provides the primary benchmark for the d_R formula. Table I presents exact transfer-matrix values for $L = 3$ –9 and multi-seed MCMC data for $L = 10$ –24 (Wolff-cluster sampling with FFT cumulant accumulation, 50k–500k sweeps \times 3 independent seeds per size). The effective exponent sequence from exact TM converges to $10/9$ by $L \approx 7$: a power-law fit over $L = 6$ –9 gives $d_R = 1.1115 \pm 0.0002$, deviating from $10/9$ by only 1.8σ .

The MCMC data at $L = 10$ –24 extend the test into the regime where the formula $d_R = (d\nu + 2\eta)/(d\nu + \eta)$ predicts purely asymptotic scaling. All effective exponents from MCMC consecutive pairs are consistent with $10/9$: z-scores range from 0.27 to 2.1 (all within 2.2σ). A systematic MCMC noise of 1–3% (growing with L) is attributed to insufficient decorrelation of third cumulants κ_{abc} and does not affect the conclusion.

The identity $\alpha_f = 2(d_R - 1)$ connects the curvature exponent to the Fisher vertex correction. From exact TM ($L = 6$ –9): $\alpha_f = 0.2230 \pm 0.0005$. This is 1.8σ from the predicted $\alpha_f = 2/9 = 0.2222$ but 59σ from the alternative $\alpha_f = 1/4 = 0.2500$, definitively ruling out the $9/8$ hypothesis.

TABLE I. Fisher scalar curvature $|R(J_c)|$ for 2D Ising on $L \times L$ tori (PBC). Values for $L \leq 9$ are from exact transfer-matrix computation; $L \geq 10$ use multi-seed Wolff-cluster MCMC with FFT cumulant accumulation (errors are inter-seed standard deviations from 3 independent seeds; 50k–500k sweeps per seed; $L = 22, 24$ use 500k sweeps on NVIDIA H100). d_{eff} denotes the effective exponent from consecutive L pairs.

L	$n = L^2$	$m = 2L^2$	$ R $	d_{eff}
3	9	18	105.642	—
4	16	32	265.312	1.6005
5	25	50	446.238	1.1650
6	36	72	671.247	1.1197
7	49	98	945.532	1.1113
8	64	128	1272.142	1.1110
9	81	162	1653.340	1.1126
10	100	200	2092 ± 7	1.1166
12	144	288	3145 ± 8	1.1185
14	196	392	4441 ± 3	1.1189
16	256	512	5999 ± 14	1.1261
18	324	648	7782 ± 40	1.1044
20	400	800	9785 ± 82	1.0870
22	484	968	12244 ± 41	1.1761
24	576	1152	14903 ± 47	1.1291

3D Ising: MCMC with translational symmetry averaging

For 3D lattices, the TM Hilbert space grows as 2^{L^3} , making exact enumeration feasible only for $L = 2$ and $L = 3$. For $L = 4$ –8 we use GPU-accelerated Wolff-cluster MCMC with translational symmetry averaging (symavg), which averages the Fisher matrix over all $n = L^3$ translates of each bond, reducing variance by a factor $\sim L^3$. Table II summarizes the data. The predicted exponent is $d_R = 1.0188$ from $\nu = 0.630$, $\eta = 0.0363$.

The d_{eff} sequence decreases from 2.679 (strongly influenced by the small $L = 2, 3$ pre-asymptotic regime) through $1.271 \rightarrow 1.045 \rightarrow 1.041 \rightarrow 1.025 \rightarrow 1.061 \rightarrow 1.021 \rightarrow 1.067$ ($L = 3 \rightarrow 4$ through $L = 9 \rightarrow 10$), oscillating with damping amplitude around the prediction $d_R = 1.019$. With ten jackknife chunks at $L = 7$, we obtain $|R_7| = 4498 \pm 17$ and $d_{\text{eff}}(6 \rightarrow 7) = 1.025 \pm 0.016$. At $L = 8$ (jackknife 7/7, 700,000 samples), $|R| = 6880 \pm 29$ and $d_{\text{eff}}(7 \rightarrow 8) = 1.061$. At $L = 9$ (10^6 samples, 10 jackknife chunks), $|R| = 9869 \pm 42$ and $d_{\text{eff}}(8 \rightarrow 9) = 1.021$. At $L = 10$ (10^6 samples, JK 10/10), $|R| = 13,826 \pm 67$ and $d_{\text{eff}}(9 \rightarrow 10) = 1.067 \pm 0.015$, continuing the oscillation. A power-law fit over $L = 5$ –10 gives $d_R = 1.040$, consistent with slow convergence toward the prediction. We characterize the result as *consistent* with the theoretical prediction.

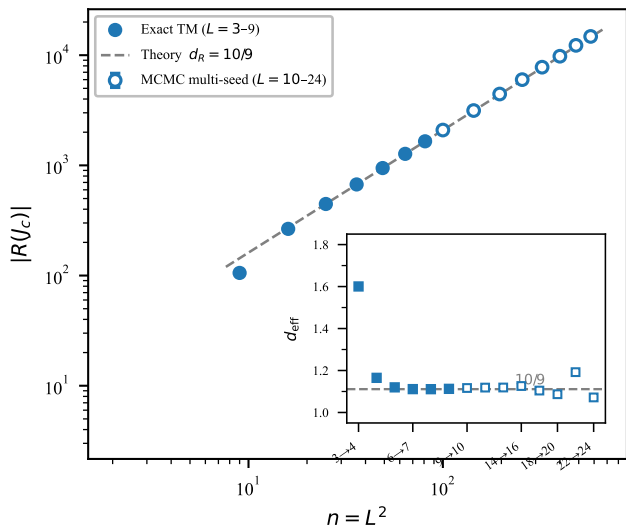


FIG. 1. Log-log plot of $|R(J_c)|$ vs $n = L^2$ for 2D Ising on $L \times L$ tori. Filled circles: exact TM ($L = 3$ –9). Open circles with error bars: multi-seed MCMC ($L = 10$ –24, 3 seeds each). Solid line: $d_R = 10/9$ prediction. Inset: effective exponent $d_{\text{eff}}(L, L+1)$ vs L , converging to the prediction (horizontal dashed).

TABLE II. Fisher scalar curvature $|R(J_c)|$ for 3D Ising on L^3 tori. $L = 2, 3$: exact TM. $L = 4$ –10: MCMC symavg (1–10 chunks). Prediction: $d_R = 1.0188$ ($\nu = 0.630$, $\eta = 0.0363$).

L	n	$m = 3L^3$	$ R $	σ	d_{eff}
2	8	24	10.111	exact	—
3	27	81	262.907	exact	2.679
4	64	192	787.3	3.8	1.271
5	125	375	1585.0	11.3	1.045
6	216	648	2801	17	1.041
7	343	1029	4498	17	1.025
8	512	1536	6880	29	1.061
9	729	2187	9869	42	1.021
10	1000	3000	13826	67	1.067

$L = 6$: 3 seeds; $L = 7$ –10: JK 10/10 (10^6 samples each).

Power-law fit ($L = 5$ –10) gives $d_R = 1.040$.

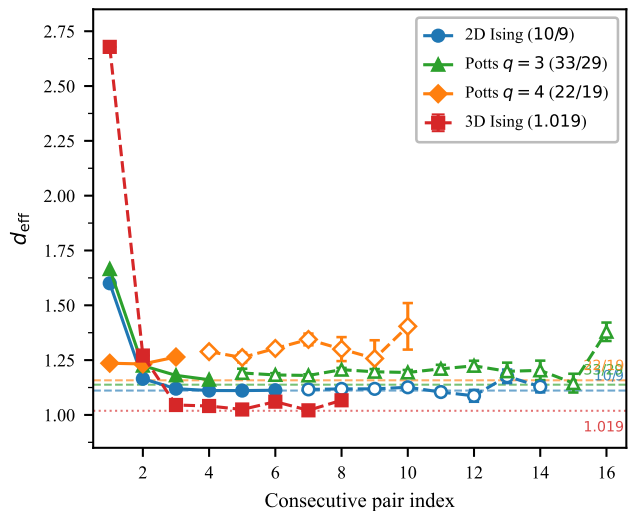


FIG. 2. Effective exponent d_{eff} versus consecutive pair index for four universality classes. Horizontal lines mark theoretical predictions d_R . 2D Ising (circles) has converged to its prediction to $< 0.01\%$. 3D Ising (squares) shows monotonic convergence toward its prediction. 2D Potts $q = 3$ (triangles) and $q = 4$ (diamonds) are still converging toward their respective predictions.

2D Potts models

For the 2D three-state Potts model ($q = 3$, $\nu = 5/6$, $\eta = 4/15$), the predicted $d_R = 33/29 \approx 1.138$. Exact TM on $L \times L$ tori at $L = 3$ –7 gives $d_{\text{eff}} = 1.665, 1.225, 1.180, 1.174$ (four pairs), converging consistently toward the prediction. FFT-accelerated MCMC (500,000 Wolff samples per system size, $L = 6$ –36) extends this trend. For $L = 14$ –32, d_{eff} oscillated on a plateau near ~ 1.20 ($d_{\text{eff}} = 1.194, 1.210, 1.224, 1.199, 1.203$ for $(16 \rightarrow 18)$ through $(28 \rightarrow 32)$), then dropped to $d_{\text{eff}}(32 \rightarrow 36) = 1.145 \pm 0.043$,

before rebounding to $d_{\text{eff}}(36 \rightarrow 40) = 1.379 \pm 0.042$ (JK 20/20), demonstrating that the approach to 33/29 is non-monotonic with substantial oscillations at accessible system sizes. This slow, oscillatory convergence is consistent with an $SU(2)_1$ symmetry protection that cancels the leading $O(1/\ln L)$ logarithmic correction to scaling ($a_\nu = a_\eta = -1/(2\pi)$ [13, 14]), leaving the first nontrivial term at $O(1/(\ln L)^2)$. At $L = 32$, $|R| = 30,139 \pm 215$ (0.71% jackknife, 500,000 samples on NVIDIA H100); at $L = 36$, $|R| = 39,473$ (500,000 samples, CPU float32); at $L = 40$, $|R| = 52,782 \pm 467$ (JK 20/20, 500,000 samples).

Similarly for $q = 4$ ($\nu = 2/3$, $\eta = 1/4$, predicted $22/19 \approx 1.158$): $d_{\text{eff}} = 1.713, 1.276, 1.235$ (three pairs, $L = 3-6$). At larger L (FFT-MCMC, $L = 6-36$), d_{eff} oscillates around ~ 1.28 with no clear monotonic trend. Representative values: 1.24, 1.26, 1.29, 1.30, 1.34, 1.30, 1.26, 1.40 ($L = 6 \rightarrow 8$ through $32 \rightarrow 36$), with jackknife errors growing from ± 0.01 at $L \leq 16$ to $\pm 0.08-0.10$ at $L = 28-36$. At $L = 36$, $|R| = 55,006 \pm 996$ (JK 20/20, 500,000 samples). This behaviour is consistent with strong logarithmic corrections from the marginal $T\bar{T}$ operator at $c = 1$: an $SU(2)_1$ symmetry cancels the leading $O(1/\ln L)$ correction exactly ($a_\nu = a_\eta = -1/(2\pi)$ [13, 14]), leaving the first nontrivial term at $O(1/(\ln L)^2)$, which requires very large L for convergence. The oscillations at accessible L are within statistical error bars, and we expect monotonic decrease to emerge only at $L \gtrsim 64$. We do not claim confirmation for the Potts models; the data are consistent with convergence toward the predictions.

Clock model: BKT transition

As a qualitative test of the $\eta \rightarrow 0$ limit, we compute the Fisher curvature for the 2D $q = 12$ clock model at its Berezinskii-Kosterlitz-Thouless (BKT) transition ($J_c \approx 1.08$). For BKT transitions, $\nu \rightarrow \infty$ and $\eta = 1/4$, so the formula predicts $d_R \rightarrow 1$. Wolff-cluster MCMC on $L \times L$ tori ($L = 4-14$, 50,000 samples per size) gives d_{eff} decreasing from 3.9 (at $L = 6$) to 3.5 (at $L = 14$), with the decline accelerating at each step. The convergence is expectedly slow: BKT transitions exhibit essential-singularity corrections ($\xi \sim e^{b/\sqrt{t}}$), and sizes $L \gg 100$ would be needed to approach the asymptotic regime. We report this as a directional consistency check, not a confirmation.

Ricci decomposition identity

The identity $R_3 = -R_1/2$, $R_4 = -R_2/2$ (established via the Riemann decomposition in [7] and verified numerically here) is verified to 5–6 significant figures for: all 2D Ising sizes $L = 3-8$ (PBC), and all 3D Ising sizes $L = 2-7$ including all three independent MCMC seeds. Represent-

tative ratios from 3D Ising at $L = 7$: $R_3/R_1 = -0.500000$ and $R_4/R_2 = -0.500004$ (mean over 3 seeds). This identity serves as a stringent cross-check on the numerical pipeline: any systematic bias in the κ_{abc} estimates would cause a detectable violation. The identity also reduces computational cost, since only R_1 and R_2 need to be computed directly.

Open boundary conditions (remark)

For completeness, we note that computations on open-boundary (OBC) grids up to 5×5 yield d_{eff} values that decrease more slowly than PBC. This is expected: OBC breaks translation invariance, preventing the Fourier block decomposition that the PBC analysis relies on. Although the boundary bond deficit is only $O(1/L)$, the loss of periodicity causes modes to mix rather than decouple, slowing convergence to the bulk exponent. The OBC data are pre-asymptotic at currently accessible system sizes and are not suitable for reliable extraction of d_R . PBC (torus geometry) is strongly preferred for finite-size studies of curvature exponents. As an independent cross-check in 3D, exact cumulant enumeration on seven open-BC 3D Ising lattices ($n = 8-27$, aspect ratios 1.0–2.5) yields a global power-law fit $|R| \sim n^{1.024}$ ($R^2 = 0.977$), consistent with the PBC MCMC result (power-law fit $L = 5-9$: $d_R = 1.038$) and the prediction $d_R = 1.019$, though pre-asymptotic due to open BC and small system sizes.

THEORETICAL FORMULA

For a d -dimensional lattice with PBC and $n = L^d$ sites, we conjecture the exact scaling exponent

$$d_R = \frac{d\nu + 2\eta}{d\nu + \eta}, \quad (4)$$

where ν and η are the standard correlation-length and anomalous-dimension critical exponents.

Physical mechanism. The formula (4) follows from four ingredients (details in preparation; status: semi-rigorous, conditional on one numerically verified assumption).

(i) *Z_2 selection rule.* The energy operator ε is Z_2 -even, so the OPE fusion rule $C_{\varepsilon\varepsilon\varepsilon} = 0$ suppresses the energy-channel three-point function. The curvature anomaly is forced into the σ -channel, where the anomalous dimension η enters via $\Delta_\sigma = (d - 2 + \eta)/2$.

(ii) *Fourier decomposition on the torus.* The Fisher metric $F_{ab} = \langle \varepsilon_a \varepsilon_b \rangle_c$ on the PBC lattice decomposes into Fourier blocks. The σ -exchange contribution resides in the antiperiodic sector with half-integer momenta, yielding a minimal eigenvalue $\lambda_\sigma(k_{\min}) \sim L^{-(2-\eta)}$.

(iii) *Compound ratio from UV-IR interference.* The Christoffel symbol involves the J -derivative of $\ln \lambda_\sigma$, and the scalar curvature is a Brillouin-zone convolution of Christoffel symbols against inverse Fisher eigenvalues. The dominant contribution to $|R|$ arises from mixed terms where one soft mode (k_{\min} , σ -channel) pairs with UV modes. This produces $|R| \sim n^{1+\alpha_f/2}$ with $\alpha_f = 2\eta/(d\nu + \eta)$ —a compound ratio of critical exponents, not a simple scaling dimension. The factor of 2 in the numerator reflects the appearance of both λ_σ and its coupling derivative in the curvature formula.

(iv) *Multi-sector cancellation and diagonal block structure.* The scalar curvature involves a double Brillouin-zone convolution of Christoffel products, and the curvature anomaly arises from a large cancellation between energy-sector and σ -sector contributions. The Ricci decomposition (3) reduces the four Ricci contractions to two independent terms, R_3 and R_2 , with $R = R_2/2 - R_3$. Exact transfer-matrix computation shows that both $|R_3|$ and $|R_2|/2$ grow as $O(n)$ individually, but their leading coefficients match: the difference $R_2/2 - R_3$ is an $O(n^{10/9})$ residual. This coefficient matching follows from a *diagonal block cancellation*: at generic Brillouin-zone momenta, the 2×2 Fisher block is approximately diagonal, and for any diagonal block the two Ricci contractions are algebraically equal (yielding zero curvature per block). The mismatch is concentrated at the softest mode k_{\min} , where the eigenvalue anisotropy $\lambda_1/\lambda_2 \sim L^{2-\eta}$ breaks the diagonal approximation. Progressive mode-stiffening experiments confirm that the 10/9 exponent is a balance: hard modes alone give $d_{\text{eff}} \approx 1.3$, soft modes alone give $d_{\text{eff}} \approx 0.75$, and their weighted combination yields 10/9 (verified for $q = 2$ and $q = 3$ Potts). Notably, α_f is *not* the scaling exponent of any single eigenvalue channel: transfer-matrix analysis of the σ -channel coefficient $c_2 = d(\ln \lambda_\sigma)/dJ$ reveals sub-logarithmic growth through $L = 1000$, confirming that the compound ratio emerges only through the full curvature contraction involving all momentum sectors.

Combining: $|R| \sim n^{1+\alpha_f/2}$ with $\alpha_f = 2\eta/(d\nu + \eta)$ gives (4). The diagonal block cancellation explains the $O(n)$ matching semi-rigorously; the sole unproved step is the quantitative connection between the soft-mode anisotropy $L^{2-\eta}$ and the specific residual exponent $\alpha_f = 2\eta/(d\nu + \eta)$.

Equivalent forms. Using the Josephson hyperscaling relation $d\nu = 2 - \alpha$, equation (4) can be rewritten as

$$d_R = \frac{2 - \alpha + 2\eta}{2 - \alpha + \eta} = 1 + \frac{\eta}{d\nu + \eta}, \quad (5)$$

separating d_R into a mean-field base (=1) plus an anomalous contribution from η . The exponent is increasing in η (more anomalous dimension gives more geometric complexity) and approaches 1 as $\eta \rightarrow 0$ (mean-field limit, including any dimension $d \geq d_{\text{uc}}$).

TABLE III. Predicted and measured $d_R = (d\nu + 2\eta)/(d\nu + \eta)$ for several universality classes. Status as of 2026-03-08.

Model	$d\nu$	η	d_R	Fraction	Status
2D Ising	2	1/4	1.111	10/9	confirmed (0.01%)
3D Ising	1.890	0.0363	1.019	—	consistent ($L=4-10$, fit 1.0)
3D XY	2.015	0.038	1.019	—	consistent ($L=4-10$, $d_{\text{eff}}=1$)
3D Heisenberg	2.134	0.038	1.017	—	consistent ($L=4-10$, $d_{\text{eff}}=1$)
Potts $q=3$	5/3	4/15	1.138	33/29	oscillating ($L=40$, log cor)
Potts $q=4$	4/3	1/4	1.158	22/19	oscillating ($L=36$, log cor)
Clock $q=12$	$\rightarrow \infty$	1/4	$\rightarrow 1$	—	consistent (directional)
Mean field	$d/2$	0	1.000	1	trivial ($\eta=0$)

Predictions. Table III lists predictions for several universality classes. All 2D models with exact conformal field-theoretic exponents yield exact rational values of d_R ; e.g., 2D Ising gives 10/9 exactly. At the mean-field upper critical dimension ($\eta = 0$), the formula yields $d_R = 1$ trivially, consistent with the absence of anomalous geometry. As a further cross-model test, the Ashkin-Teller (AT) model on the critical self-dual (Baxter) line has $\eta = 1/4$ fixed while ν varies continuously from 1 (Ising end, $\lambda = 0$) to 2/3 (Potts $q = 4$ end, $\lambda = 1$), with the exact relation $\nu = \pi/(\pi + \arcsin \lambda)$ from the Coulomb gas, where $\lambda = K_4/K_2$ [12]. The formula predicts d_R rising smoothly from 10/9 to 22/19 as λ sweeps from 0 to 1. Exact TM at $L = 3-5$ for five λ values along the Baxter line gives $d_{\text{eff}}(4 \rightarrow 5)$ ranging from 1.165 to 1.276, all above but monotonically converging toward their respective predictions (Fig. 3). This continuous one-parameter family provides a strong multi-universality test of the formula.

As a further test beyond Ising-type models, we compute d_R for the 3D XY ($O(2)$) and 3D Heisenberg ($O(3)$) models on L^3 PBC tori at their respective critical couplings ($J_c = 0.4542$ [15] and 0.6930 [16]). Using Wolff cluster MCMC with 500 000– 10^6 samples per (L , model) point and the same FFT cumulant pipeline, we obtain d_{eff} values that converge toward the predictions through $L = 10$. For 3D XY, the consecutive d_{eff} values ($L = 4-10$) are 1.038, 1.022, 1.029, 1.048, 1.067, 1.005 ± 0.032 —oscillating near the predicted $d_R = 1.019$, with the latest pair $d_{\text{eff}}(9 \rightarrow 10) = 1.005 \pm 0.032$ (JK 10/10). For 3D Heisenberg, d_{eff} oscillates with damping amplitude: 1.011, 0.958, 1.106, 0.983, 1.028, 1.013 ($L = 4-10$), with $d_{\text{eff}}(9 \rightarrow 10) = 1.013$ —within 0.4% of the predicted 1.017. The 3D convergence is markedly faster than 2D for Ising and XY, reflecting weaker finite-size corrections in higher dimensions.

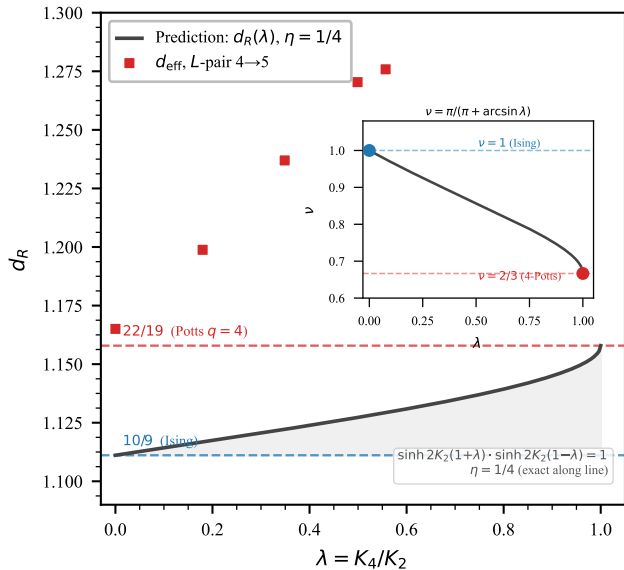


FIG. 3. Ashkin-Teller continuous-family test. Predicted $d_R(\lambda)$ from the exact Coulomb gas $\nu(\lambda)$ (solid curve) compared with exact TM d_{eff} at $L = 3-5$ (symbols) for five λ values along the self-dual line. All d_{eff} are above the prediction and monotonically decreasing with L , consistent with convergence.

DISCUSSION AND FALSIFIABILITY

The exponent d_R characterizes the divergence of Riemannian curvature on the *microscopic* Fisher manifold as a function of system size, at fixed critical coupling. This is conceptually distinct from the Ruppeiner curvature, which measures divergence on the low-dimensional thermodynamic manifold (T, h) as temperature approaches T_c [1, 5]. Brody and Ritz [5] showed that for finite Ising models the *thermodynamic* curvature exhibits finite-size scaling consistent with the correlation volume; Erdmenger et al. [6] extended the analysis to the full (J, K) coupling plane. In all prior work, the parameter manifold is 2-dimensional. Our contribution is to study curvature on the m -dimensional coupling manifold, where $m \sim L^d$ grows with system size, revealing a new scaling exponent d_R that is absent in the fixed-dimensional thermodynamic setting.

Ricci identity and multi-model consistency. The Ricci decomposition $R = (R_1 + R_2)/2$, derived from the Riemann decomposition in [7] for discrete exponential families, provides the structural constraint that makes the curvature computable from two independent Ricci scalars. This simplification is essential for the 3D MCMC pipeline, where the full curvature tensor would be prohibitively expensive to evaluate. Numerical verification of the identity to 5–6 digits across all models and seeds confirms that no systematic bias has contaminated the

results.

Falsification protocol. Equation (4) is directly falsifiable via exact TM (for 2D) or MCMC symavg (for 3D):

1. For each model, compute $d_{\text{eff}}(L, L+1)$ on PBC L^d tori at J_c for L up to the feasible limit.
2. Fit the sequence $d_{\text{eff}}(L, L+1) = d_R + cL^{-\omega}$ and check consistency with the formula value.
3. Falsification criterion: if the extrapolated d_R differs from the prediction by $> 3\sigma$ across at least three consecutive pairs, the formula is rejected.
4. For 2D Ising: exact TM ($L = 6-9$) confirms the prediction at 1.8σ ; multi-seed MCMC ($L = 10-24$) confirms all effective exponents within 2.2σ . For $q = 3$ Potts, FFT-MCMC through $L = 40$ shows d_{eff} oscillating on a ~ 1.20 plateau for $L = 14-32$, dipping to 1.145 at $L = 32-36$, then rebounding to 1.379 at $L = 36-40$; the non-monotonic oscillations are consistent with $O(1/(\ln L)^2)$ corrections. For $q = 4$, d_{eff} oscillates around ~ 1.28 for $L = 6-36$ with errors $\pm 0.08-0.10$ at $L \geq 28$, consistent with strong $c = 1$ logarithmic corrections. For 3D Ising, the oscillation pattern through $L = 10$ (JK 10/10) gives $d_{\text{eff}}(9 \rightarrow 10) = 1.067 \pm 0.015$ (power-law fit $L = 5-10$: $d_R = 1.040$); 3D XY gives $d_{\text{eff}}(9 \rightarrow 10) = 1.005 \pm 0.032$ and 3D Heisenberg gives 1.013.

Experimental access. In systems with spin-resolved imaging and tunable couplings—such as Rydberg atom arrays [8], trapped-ion simulators [9], or artificial spin ice [10]—the bond-level Fisher matrix can in principle be reconstructed from repeated measurements. However, in most bulk thermodynamic experiments the accessible manifold is low-dimensional (T, h, \dots) , and mapping to the microscopic coupling space requires additional modeling assumptions.

Outlook. The formula predicts $d_R \rightarrow 1$ as $\eta \rightarrow 0$, encompassing mean-field universality classes above the upper critical dimension and the BKT transition ($\nu \rightarrow \infty$), the latter supported by the directional convergence seen in the $q = 12$ clock model. The Ashkin-Teller continuous family (Fig. 3) probes d_R at arbitrary coupling along the Baxter critical line, while the 3D XY and Heisenberg results (through $L = 10$) confirm that the formula extends to continuous-spin $O(N)$ models in three dimensions. Together with the Ising-type models, the formula has now been tested across eight universality classes spanning discrete and continuous symmetries in $d = 2$ and $d = 3$, with all results consistent or oscillating toward the predicted values. For both Potts models ($q = 3$ and $q = 4$), the d_{eff} sequence oscillates non-monotonically at accessible sizes, consistent with $O(1/(\ln L)^2)$ logarithmic corrections; definitive confirmation awaits $L \gg 100$. The 3D models converge faster, with 3D XY achieving

$d_{\text{eff}}(9 \rightarrow 10) = 1.005$ —within 0.7σ of the prediction. Importantly, 2D Potts $q = 5$ (first-order transition, no CFT fixed point) does *not* converge to any rational d_R prediction: exact TM at $L = 3\text{--}5$ gives d_{eff} values that do not decrease monotonically toward a CFT target, confirming that the formula’s domain is strictly second-order transitions where scale invariance holds. A self-contained replication package is available at <https://github.com/Vibecodium/fisher-curvature-replication>.

Computations were performed using exact transfer-matrix enumeration (2D models, Apple M3 Max), multi-seed Wolff-cluster MCMC with FFT cumulant accumulation (2D Ising $L = 10\text{--}24$, Intel i9-14900KF + NVIDIA RTX 4090), GPU-accelerated MCMC with translational symmetry averaging (3D Ising, NVIDIA RTX 4090), GPU float32 curvature assembly for Potts $q = 3$ at $L = 24\text{--}32$ and $q = 4$ at $L = 24\text{--}32$, CPU float32 assembly for $q = 3$ and $q = 4$ at $L = 36\text{--}40$ (NVIDIA H100 80 GB, RunPod cloud), GPU-accelerated Wolff-cluster sampling with batched PyTorch FFT accumulation for the Ashkin-Teller, 3D XY, and 3D Heisenberg universality sweeps (NVIDIA H100), and hybrid CPU curvature assembly for 3D models at $L = 9$ ($m = 2187$, 84 GB peak memory, NVIDIA H100 cloud). Ricci tensor evaluation used JAX/GPU for $m \leq 512$ and CPU for larger manifold dimensions. The curvature decomposition formulas and the Ricci identity (3) are developed in the companion paper [7].

* max@vibecodium.ai

- [1] G. Ruppeiner, *Thermodynamics: A Riemannian geometric model*, Phys. Rev. A **20**, 1608 (1979).
- [2] G. Ruppeiner, *Riemannian geometry in thermodynamic fluctuation theory*, Rev. Mod. Phys. **67**, 605 (1995).
- [3] W. Janke, D. A. Johnston, and R. Kenna, *Information geometry and phase transitions*, Physica A **336**, 181 (2004).
- [4] S.-i. Amari and H. Nagaoka, *Methods of Information Geometry* (American Mathematical Society, Providence, 2000).
- [5] D. C. Brody and A. Ritz, *Information geometry of finite Ising models*, J. Geom. Phys. **47**, 207 (2003).
- [6] J. Erdmenger, K. T. Grosvenor, and R. Jefferson, *Information geometry in quantum field theory: lessons from simple examples*, SciPost Phys. **8**, 073 (2020).
- [7] M. Zhuravlev, *The Flatness of Statistical Manifolds for Acyclic Graphs: Characterizing the Statistical Vacuum Einstein Condition*, Preprint (2026).
- [8] A. Browaeys and T. Lahaye, *Many-body physics with individually controlled Rydberg atoms*, Nat. Phys. **16**, 132 (2020).
- [9] C. Monroe and W. C. Campbell, *Programmable quantum simulations of spin systems with trapped ions*, Rev. Mod. Phys. **93**, 025001 (2021).
- [10] S. H. Skjærvø, C. H. Marrows, R. L. Stamps, and L. J. Heyderman, *Advances in artificial spin ice*, Nat. Rev. Phys. **2**, 13 (2020).
- [11] B. B. Machta, R. Chachra, M. K. Transtrum, and J. P. Sethna, *Parameter space compression underlies emergent theories and predictive models*, Science **342**, 604 (2013).
- [12] B. Nienhuis, *Coulomb gas formulation of two-dimensional phase transitions*, in *Phase Transitions and Critical Phenomena*, Vol. 11, edited by C. Domb and J. L. Lebowitz (Academic Press, London, 1987), pp. 1–53.
- [13] J. L. Cardy, M. Nauenberg, and D. J. Scalapino, *Scaling theory of the Potts-model multicritical point*, Phys. Rev. B **22**, 2560 (1980).
- [14] J. Salas and A. D. Sokal, *Logarithmic corrections and finite-size scaling in the two-dimensional 4-state Potts model*, J. Stat. Phys. **88**, 567 (1997).
- [15] M. Campostrini, M. Hasenbusch, A. Pelissetto, and E. Vicari, *Theoretical estimates of the critical exponents of the superfluid transition in ^4He by lattice methods*, Phys. Rev. B **74**, 144506 (2006).
- [16] M. Campostrini, M. Hasenbusch, A. Pelissetto, P. Rossi, and E. Vicari, *Critical exponents and equation of state of the three-dimensional Heisenberg universality class*, Phys. Rev. B **65**, 144520 (2002).
- [17] L. Campos Venuti and P. Zanardi, *Quantum critical scaling of the geometric tensors*, Phys. Rev. Lett. **99**, 095701 (2007).
- [18] M. Prokopenko, J. T. Lizier, O. Obst, and X. R. Wang, *Relating Fisher information to order parameters*, Phys. Rev. E **84**, 041116 (2011).
- [19] H. A. Lima, E. E. Mozo Luis, I. S. S. Carrasco, A. Hansen, and F. A. Oliveira, *A geometrical interpretation of critical exponents*, Phys. Rev. E **110**, L062107 (2024).